

Review

Not peer-reviewed version

Martian Dust Storms: Reviews and Perspective for Tianwen-3 Mars Sampling Returning Mission

[Fei He](#)*, Zhaojin Rong, Zhaopeng Wu, Jiawei Gao, Kai Fan, [Xu Zhou](#), Limei Yan, Yuqi Wang, Yong Wei

Posted Date: 31 May 2024

doi: 10.20944/preprints202405.2105.v1

Keywords: Mars; Dust Storm; Remote Sensing; Monitor and Forecast; Tianwen-3



Preprints.org is a free multidiscipline platform providing preprint service that is dedicated to making early versions of research outputs permanently available and citable. Preprints posted at Preprints.org appear in Web of Science, Crossref, Google Scholar, Scilit, Europe PMC.

Copyright: This is an open access article distributed under the Creative Commons Attribution License which permits unrestricted use, distribution, and reproduction in any medium, provided the original work is properly cited.

Review

Martian Dust Storms: Reviews and Perspective for Tianwen-3 Mars Sampling Returning Mission

Fei He ^{1,2,*}, Zhaojin Rong ^{1,2}, Zhaopeng Wu ¹, Jiawei Gao ^{1,2}, Kai Fan ¹, Xu Zhou ¹, Limei Yan ^{1,2}, Yuqi Wang ¹ and Yong Wei ^{1,2}

¹ Key Laboratory of Earth and Planetary Physics, Institute of Geology and Geophysics, Chinese Academy of Sciences, Beijing, China;

² College of Earth and Planetary Sciences, University of Chinese Academy of Sciences, Beijing, China;

* Correspondence: hefei@mail.iggcas.ac.cn;

Abstract: Dust storms play a crucial role in the climate system and the space environment of Mars and have a great impact on human's Mars exploration activities. The Martian dust storms exhibit significant regional, seasonal and interannual variations due to various controlling factors such as the large-scale atmospheric circulation, varying solar radiation forcing, and Martian orbital and rotational motions and their coupling to the atmospheric dynamics. This paper focuses on the review of current understandings on Martian dust storms. This paper begins by elucidating the basic properties of dust storms, and their driving mechanisms and impacts on atmospheric dynamics, atmospheric electric property, space environment, topography, and Mars explorations. Then it introduces the observation methods on different platforms including orbiters and landers/rovers, and the datasets constructed based on these historical observations for Martian dust storms. Finally, we proposed the dust storm monitoring and forecasting for the upcoming Chinese Tianwen-3 Mars sampling returning mission. It concludes by depicting the future research topics to systematically understand the Martian dust storms.

Keywords: Mars; Dust Storm; Remote Sensing; Monitor and Forecast; Tianwen-3

1. Introduction

Mars is the fourth terrestrial planet and the second smallest planet in the solar system after Mercury. Mars is named after the God of War in ancient Roman mythology and is also known as the "Red Planet" since its surface is covered with hematite. The radius of Mars is 3390 km, significantly smaller than Earth. The aphelion and perihelion of Mars orbit are 1.666 AU (1 AU $\approx 1.5 \times 10^8$ km) and 1.381 AU, respectively, with an eccentricity of 0.933941 and a sidereal orbital period of 686.98 Earth days. In ancient Chinese, Mars is called "yíng huò (荧惑)" because it glows like fire and its position and brightness often change. Mars is lack of global dipolar magnetic field [1] and has lost most of its atmosphere to space over billions of years [2]. Present Mars is frigid and arid since most of water has escaped through multiple processes which are influenced by several factors [3–9], such as solar wind variations, solar extreme ultraviolet (EUV) radiations, and dust storms.

Without a protective global dipolar magnetic field and the persistent escape, the atmosphere of Mars is very thin and cold, and the surface atmospheric pressure is just 0.6% of the Earth. The Martian atmosphere is dominated by carbon dioxide (95.3%) [10]. The large difference between the aphelion and perihelion of Mars orbit generates clear seasonal variations in Mars climate and environment variations. The seasonal cycle of the sublimation and condensation of carbon dioxide in polar regions of Mars results in the changes in surface atmospheric pressure of up to 20% [11]. The high eccentricity of Mars orbit also causes a dramatic variation in solar radiations of up to 30% on Mars during one Martian year [12].

The surface of Mars is full of river channels, canyons, ravines, alluvial plains, and other features. Research suggests that Mars may have once been a habitable planet, with a global dipole magnetic field, abundant liquid water, and a dense atmosphere ~3 Gy ago [13]. Therefore, Mars has always

been the focus of human planetary exploration because it carries the dream of mankind to search for extraterrestrial life. Until now, human has launched more than fifty missions to Mars, including orbiters, landers, and rovers. These missions significantly advanced our understanding of Mars environment. For these missions, the landers and rovers are apparently affected by the Martian surface environment [14,15]. Among the many seasonal variation characteristics of Mars, the seasonal dust storm is particularly obvious, which is an important regulatory factor for the changes of Mars' climate and surface environment, space environment, and even atmospheric escape [16]. Dust storms have become the biggest threat to missions to the surface of Mars.

This paper is organized as follows. Section 2 reviews the existing research on dust storms, including their triggering mechanisms, evolution characteristics, and effects on Mars surface and space environment. In Section 3, we describe the current observations methods for dust storms. In Section 4, we present schemes for dust storm monitoring for Chinese Tianwen-3 sample return mission. The concluding remarks will be given in Section 4.

2. Mars Dust Storms

As the most dramatic activity in the Martian climate system composed of the surface and atmosphere, dust storms on Mars have significant seasonal variations. During each Mars year, as Mars approaches its southern summer solstice, local, regional, and global dust storms (Figure 1) become very active on the surface of Mars. In this section, we review the basic properties of dust storms and their impacts on Mars environment.

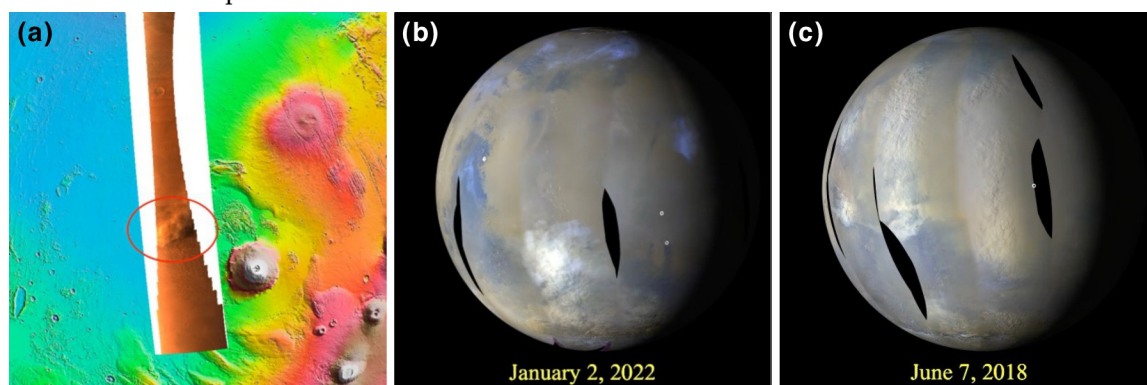


Figure 1. Illustration of local, regional, and global dust storms. (a) A local dust storm in the Amazonis Planitia near the Olympus Mountain captured by the Moderate Resolution Imaging Camera (MoRIC) onboard Tianwen-1 mission on 6 January 2022. (b) A regional dust storm in the southern hemisphere captured by the Mars Color Imager (MARCI) onboard Mars Reconnaissance Orbiter (MRO). (c) A global dust storm in 2018 captured by the MARCI onboard MRO.

2.1. Basic Properties of Dust Storms

The Martian dust storms can be categorized based on different standards. According to the scales of the dust storms, they can be categorized as local dust storms, regional dust storms, and global dust storms [17,18], as shown in Figure 1. A regional dust storm is defined as dust events occupying a spatial area $\geq 1.6 \times 10^6$ km² and a duration longer than 2 days. The lofted dust can travel great distances, even around Mars in a latitude zone, and be deposited far away from the source region. Isolated dust events with smaller sizes or shorter durations are classified into local dust storms which generally last less than 3 days. Global dust storms are also referred as planet encircling dust storms which sweep the Martian globe. The rapid expansion and combination of multiple local and regional dust storms finally become a global dust storm which usually continues tens of days.

The local dust storms can occur in any season at any place on Mars. Regional dust storms are common during southern hemisphere spring and summer seasons, with a solar longitude (L_s) range between 180° and 360°. The dust storms occur in preferred locations, such as Acidalia, Utopia, Arcadia, and Hellas [19]. The global dust storms are unpredictable nonperiodic events, both in time and

location. Only few confirmed global dust storms were observed in years 1956, 1971, 1973, 1977, 2001, 2007, 2018 [20].

In terms of season and time scale, Martian regional-scale dust storms can be divided into three types: A, B and C [21], and an example in Martian year 36 is shown in Figure 2 (please refer to Section 3 for the details of column dust optical depth (CDOD) [22,23]). Their active time is generally in the southern hemisphere spring and summer seasons (L_s range 180° – 360°), while the southern hemisphere autumn and winter seasons (L_s range 0° – 180°) are generally a calm period of dust activity. Type A dust storms generally intensify in the middle and low latitudes after the southern hemisphere spring equinox in each Martian year ($L_s=180^\circ$), covering more than two-thirds of the latitude of Mars and lasting for about four months. Type A dust storms generally have the longest duration, widest coverage, and highest intensity, and in some Martian years even evolved into global dust storms (such as 2001, 2007, 2018), and have the most significant impact on Mars exploration activities. Nearly at the end of Type A dust storm, near the summer solstice in the southern hemisphere, Type B dust storms will erupt in the south polar region of Mars, lasting about two months. Type B dust storms are mainly local and regional, and the scope of activity is mainly limited to the high latitude region near the South Pole (south of 60° S). After the end of type A and B dust storms, type C dust storms will occur in the middle and low latitudes (around $L_s=330^\circ$), lasting about one to two months and may be developed into global dust storms, ending before the southern hemisphere autumn equinox, returning to a calm state, and entering the cycle of the next Martian year.

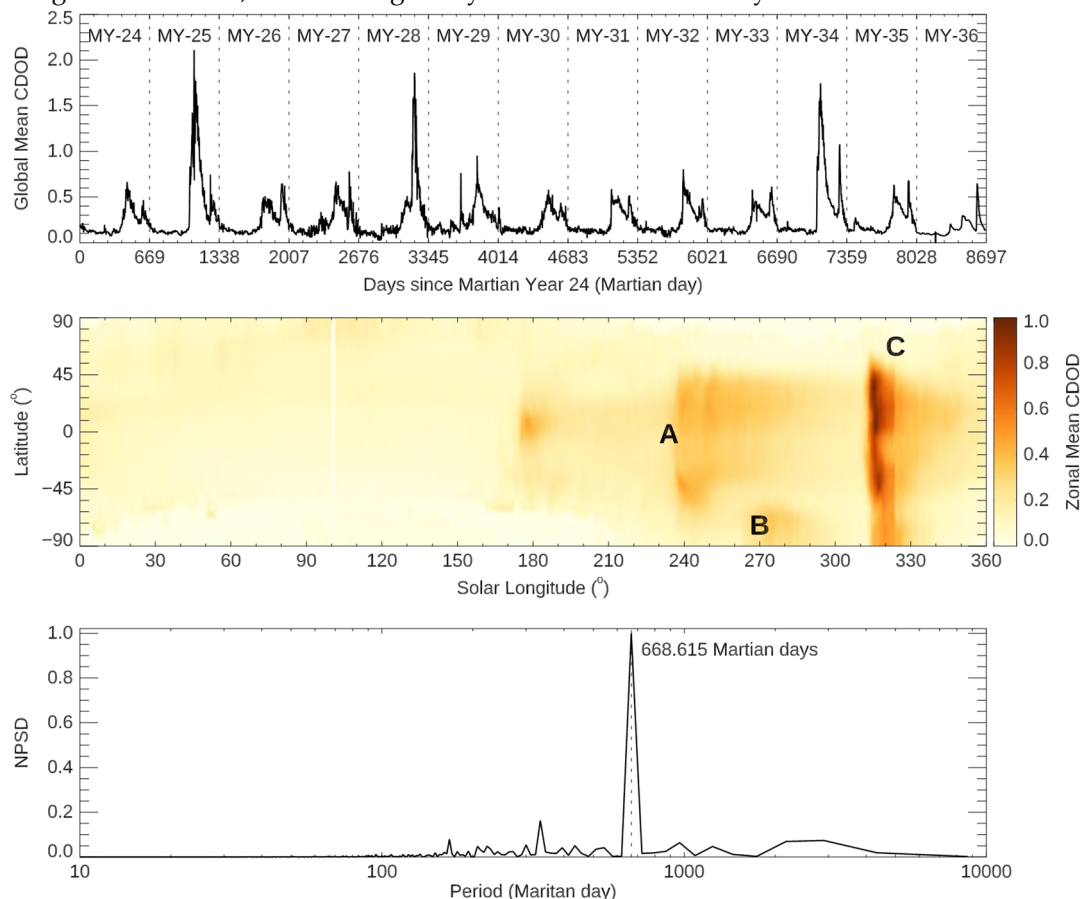


Figure 2. Zonal mean variation of absorption column dust optical depth (CDOD) on Mars. (a) Temporal variations of the global mean CDOD from Martian year 24 to 36. (b) An example of zonal mean $9.3\ \mu\text{m}$ CDOD during Martian year 36. (c) Normalized power spectral density (NPSD) in Fourier analysis of the time series of global mean CDOD from Martian year 24 to 36.

The occurrence of Martian dust storms follows an overall seasonal pattern as described above, for example, Fourier analysis on the long-term global mean CDOD during Martian years 24–36 (Figure 2a) shows that Martian dust storms have a precise 668.615-day period (Figure 2c). However,

in different Martian years, the intensity, frequency, eruption and duration of dust storms, and their influence range all show significant irregular interannual variation characteristics, which brings great difficulty to the prediction of dust storms on Mars.

The effective radius of the lofted dust particles is near $1.5\ \mu\text{m}$ and varies from $\sim 1\ \mu\text{m}$ during weak local dust storms near Martian northern hemisphere summer solstice to $\sim 2\ \mu\text{m}$ during regional and global dust storms in Martian southern hemisphere spring and summer [24,25]. The effective radius of dust particles generally increases with the dust content in the atmosphere, that is, the particle size in southern hemisphere spring and summer is generally larger than that in southern hemisphere autumn and winter [26–28]. In the vertical direction (10–70 km height range), the distribution of dust particle size in the Martian atmosphere showed a bimodal distribution: the main peak of the particle size was $0.7\sim 1.2\ \mu\text{m}$ and the secondary peak of the particle size was $0.04\sim 0.07\ \mu\text{m}$ [29]. The altitude-dependent particle size distribution of Martian dust storms significantly affects the absorption, scattering and re-radiation of the incoming solar radiations and plays a key role in the variability of radiative balance, thus affecting large-scale atmospheric circulation and climate on Mars [30,31].

2.2. Driving Mechanisms of Dust Storms

The interannual variability of dust storms occurring in the southern hemisphere summer season significantly dominated the seasonal climate on Mars. Therefore, uncover the driving mechanisms of the dust storms is essential to understand the climate on Mars. Many mechanisms have been proposed to interpret the generation of seasonal dust storms and they may be categorized into three classes.

The first class is related with large-scale atmospheric circulation. When Mariner 9 arrived Mars in 1971, it observed for the first time in Martian orbit the decaying phase of a global encircling dust storm [32]. These observations have led to a number of efforts to understand the driving mechanisms of the global dust storm. Leovy et al. [33] reviewed such works and proposed an energy balance model. During southern hemisphere spring, dust devils and the local cyclonic dust storms [34], strong surface winds in the intense baroclinic regions [36], or the strong mass outflow wind [36] generates local dust storms, building up dust content in southern, middle and subtropical latitudes. The strong insolation, low static stability, and high atmospheric absorptivity and emissivity generate intense meridional circulations to promote the onset of a global storm [33]. Later, observations at the Viking Lander #1 indicated that the local dust storm can be caused by baroclinic wave activity with a threshold wind speed of $25\sim 30\ \text{m s}^{-1}$ [37].

Now, it is generally accepted that the seasonal dust storms are driving by the seasonally varying solar radiation forcing on the physical system consisting of the Martian surface and atmosphere. The increasing solar radiations near the southern hemisphere spring equinox heat the Mars atmosphere and accelerate atmospheric flow. The strengthened near-surface wind stress lifts the dust particles into atmosphere [38,39]. The dust particles further heat the atmosphere to generate zonal temperature gradient, which intensify the equatorial easterly, forming positive feedback in the system to lift more dust particles into the atmosphere and finally forming large regional even global dust storms.

All the regional and global dust storms are originated from local dust storms, for which the second class of mechanisms attribute dust lifting to convective vortices known as dust devils [34,38,40,41]. Gierasch and Goody [34] first proposed that an axisymmetric swirling flow field existed outside the central dusty core, and the solar radiation heating strengthened the horizontal temperature gradients to accelerate the cyclonic swirling flow inward into the core. Ryan and Lucich [40] further found that the dust devils occurred more frequently during southern hemisphere spring and summer. The coexistence of multiple dust devils has been proposed as a mechanism to generate local dust storms.

The above-mentioned mechanisms are all related to the external forcing of solar radiations. The third class of mechanism link the dust storms to the changes in Martial orbital and rotational motions and their coupling to the atmospheric dynamics [42–46]. Shirley [42] found that all the regional dust storms developed into global dust storms during periods when the orbital angular momentum of

Mars with respect to the solar system barycenter was increasing or near maximum. The latest simulations [45,46] further demonstrated that the global dust storms occur near times when orbit-spin coupling torques are peaking and near times when torques are changing most rapidly. The orbit-spin coupling generated circulatory intensification and relaxation superimposed upon the normal annual cycles of atmospheric circulation controlled by the external solar forcing. The non-synchronization of the two cycles introduces interannual variability of the dust storms [42-45].

To summary, until now, the exact mechanisms than control the interannual variations of the Martian dust storms, especially the global dust storms are still not clear. Modelling efforts achieved great success in the past decades using Mars global circulation models, such as the Mars Global Circulation Model (GCM) [38,39], the Ames Mars Global Climate Model (AMGCM) [47], with dust lifting scheme embedded. A detailed review on status of Martian whole atmosphere model and dust activities can be found in Wu et al. [48] and Zhou et al. [49]. Shirley et al. [46] recently pointed out that it is necessary to incorporate orbit-spin coupling accelerations with the above models to better reproduce the interannual variability of the Martian dust storms.

2.3. Impacts of Dust Storms

Dust activities on Mars will cause many physical and chemical effects and will bring a series of potential hazards to Mars landing exploration and manned missions. In this section, we will review the impacts of dust storms on atmospheric dynamics, atmospheric electric property, space environment, topography, and Mars explorations.

During the dust storm, the dust lifting into the atmosphere significantly absorbs solar radiation, causing the temperature of the Martian atmosphere to significantly rise at least 20 °C above the altitude of 25 km [50,51] and the drop of surface temperature. The nighttime surface temperature is raised during the main phase of dust storms, making the diurnal temperature difference significantly lower during dust storms [52]. The radiation effect of dust changes the thermal structure and dynamic conditions of the atmosphere, which further affect the atmospheric tides and intensify the meridional wind and the Hadley circulation of Mars [53,54], strengthening the interhemispheric transport of dust. Dust storms will affect the sublimation and condensation of the CO₂ ice sheet in the polar region [55], further changing the atmospheric pressure in the polar region. Apart from the strong orbital forcing on the water vapor saturation height, dust storms will significantly increase the vertical water vapor transportation, further deplete the ozone [56].

Simulations, experiments and calculations have shown that during Martian dust storms, dust driven by strong winds is easy to generate friction discharge, which excites low-frequency electromagnetic disturbances [57–60]. During periods of high dust activities, the increased dust aerosols are favorable of attaching ions, resulting in the decrease of atmosphere conductivity [61,62].

The dust activities in lower atmosphere will significantly influence the upper atmosphere, ionosphere and magnetosphere through vertical transportation and coupling. During dust storms, rising of the lower atmospheric temperature induces the increase of the density of CO₂ in the upper atmosphere [63,64]. As a result, the ionospheric peak height will be raised by tens of kilometers, but without significant variation in peak electron density [65–67]. The variations of atmospheric ion densities are species-dependent, with CO₂⁺ ions significantly increased, O⁺ ions decreased, and no obvious change in O₂⁺ ions [66]. More water vapor is transported to higher altitude during dust storms. These water molecules are dissociated and ionized, and the resultant hydrogen escape can be increased by 5–10 times [3,5,68]. At the same time, the escape rate of CO₂⁺ ions can be increased by 3 times [65].

On Mars surface, dust storms have direct impact on the topography. Dust storms can affect the deposition of dust [69] and volatile (ice/snow) [70] in the polar ice caps, which can seriously affect the analysis of Mars' climate evolution history. Dust storms can drive the redistribution of dust on Mars surface and the extremely strong winds (up to 100 km h⁻¹) play an important role in the evolution and reshaping of topography and landform []. In addition, dust storms also help to expose organic matter in the surface soil that has not been degraded by cosmic rays, which helps to assess the presence of life signals on Mars surface [72].

Apart from the environmental effects, dust storms directly impact the operations of landers and rovers on Mars surface [15]. The size of Martian dust particles ranges from 0.1 to 2000 μm , and the particles can be plate-like, angle-like, or round, with a particle density of 2.6 to 3.0 g cm^{-3} [73], and rich in Si, Al, Fe, Mg, Ca, Ti, S, Cl, Br and other elements [74]. These tiny dust particles can cover the surface of the detector or penetrate the detector, causing mechanical failure and affecting the operation of related hardware and electronics. For example, the Spirit rover lost contact in 2010 when it got stuck in the sand, preventing its solar panels from turning toward the sun. Many studies have shown that dust activities will reduce the efficiency of solar panels and even cause damages [75]. The Opportunity rover worked for fourteen years on Mars until lost contact during the 2018 global dust storm. In December 2022, the National Aeronautics and Space Administration (NASA) announced the ending of the Insight mission, which was launched in May 2018, due to the loss of power after a strong dust storm. Any landers or rovers using solar panels as power source will be significantly impacted by dust storms, even fatal damages. In addition, it was found that the Martian soil is rich in Cr (hexavalent chromium ions are highly toxic), S and Cl elements [74,76], therefore the Martian dust could be toxic and acidic, posing a significant threat to the health of astronauts. The great temperature, pressure, and wind variations during dust storms will significantly affect the entry, descending, and landing process, as well as the returning process.

In summary, dust storms have great impact on Martian environments and Mars exploration activities, comprehensive monitoring and forecasting are essential for the study of Mars multi-layer coupling system and for safe Mars exploration missions.

3. Detection Methods for Dust Storms

In 1950s, ground telescope first observed the global encircling dust storm on Mars [77]. Since then, detection and investigation of dust storms are always one of the main targets of Mars exploration missions. In this section, we review the detection methods for dust storms, with emphasis on those performed on Martian orbiters and landers.

3.1. Historical Views on Dust Storms

Before the arrival of human detectors to Mars, qualitative observation and analysis of dust storms on Mars were mainly carried out with ground-based telescopes. The interannual variation characteristics of Martian dust storms have been found, specifically, the changes in color and albedo near the perihelion of Mars indicate the frequent occurrence of large dust storms [78,79].

One of the key physical parameters to quantify the content and spatial distribution of dust particles in the Martian atmosphere is the vertical CDOD, which is related to the attenuation of light in the propagation direction caused by the absorption and scattering (i.e. extinction) of the dust particles in the atmosphere when the radiation of a specific wavelength passes through the Martian atmosphere. The larger the value is, the more serious the attenuation is and the stronger the dust activity is. The vertical profile of optical depth can be retrieved from the radiation measured by the limb observation instrument, which provides important information about the vertical transport of dust. It should be noted that while relative changes in optical depth can be easily obtained from remote sensing observations, absolute values are much more difficult to obtain, as the latter requires an accurate understanding of important properties related to dust, such as particle size distribution and optical parameters. In order to obtain the CDOD of Mars, starting with the Mariner 9 probe, most Mars probes in the United States and Europe are equipped with optical instruments that can detect dust storm activity, including spectrometers, radiometers, imagers/cameras, lidar, etc. At present, Mars dust storm monitoring methods can be roughly divided into three categories: orbiter multicolor camera, orbiter infrared spectrometer, and lander camera.

3.2. Orbiter Multicolor Imaging

Optical imaging can provide a wide range of dust storm occurrence and development trends monitoring and is the most intuitive way to monitor the dust storm activities on Mars. Two important

cameras that have been operated on Mars orbiters are the Mars Orbit Camera (MOC) onboard the Mars Global Surveyor (MGS) [80,81] and the MRO MARCI [82]. The two instruments provided Mars daily global maps from 1999 until now. These maps provided an extensive database for investigating Mars dust storms [18,19,83].

The most successful imager in Mars orbit is the MARCI onboard MRO. The MRO operated in a polar near-circular orbit of Mars, with an apogee of ~320 km and a perigee of ~255 km. At this height, large-field optical images with a spatial resolution of 1~10 m can be obtained, and with the help of Mars rotation, a global image of Mars can be obtained every day. The wave bands of MARCI cover the range from ultraviolet to visible and near-infrared band, which is selected by seven filters with central wavelengths of ~260 nm, ~320 nm, ~425 nm, ~550 nm, ~600 nm, ~650 nm, and ~725 nm, respectively. MARCI operated in a push-frame mode, the camera optical axis is always pointed at the nadir point, the cross-orbital field of view (FOV) is 180°, the FOV in another direction is 26° (visible and near infrared channel) and 20° (ultraviolet channel), and the angular resolution is 0.13°, respectively. The design of MARCI is very sophisticated, using a dual optical path single-focal plane design, and the optical system of the visible and near-infrared channel and the ultraviolet channel are independent to ensure the transmittance of different channels and optical image quality. In front of the Charge Coupling Device (CCD), two prisms were used to redirect the beams at different wavelengths to the appropriate parts of the CCD based on the principle that light with different wavelengths have different refractive indices in the same medium. More subtly, according to the focusing position of different bands on the CCD, the narrowband interference multilayer filters are directly deposited on the CCD photosensitive surface, which further realizes the narrowband filter and the suppression of light crosstalk of different wavelengths, and also realizes the simultaneous imaging of different wavelengths, which is essential for the joint scientific research of multi-band images. These ingenious designs greatly reduce the size and weight of MARCI, the volume is controlled in the order of 10 cm³, and the weight is controlled within 1 kg, which adapts to the requirements of small volume and light weight in deep space exploration.

The images of each band can be used individually to study the Martian atmosphere and surface, such as clouds, circulation, dust devils and dust storms, atmospheric ozone, polar surface processes, local albedo properties, surface color properties, mineralogical constraints, and surface physical constraints. For example, the images at wavelengths of ~425 nm, ~600 nm and ~725 nm were synthesized to obtain global color images of Mars (Figures 1b and 1c) for identifying the range and evolution path of dust storms [19], which is of great significance for revealing the generation and evolution laws of dust storms on Mars, especially the regional characteristics and space-time evolution laws of large dust storms. Based on the Mars daily global maps from MGS MOC and MRO MARCI, a comprehensive Mars dust activity database over eight Martian years (24~32) is compiled, including 14,974 dust storms with area >10⁵ km² [84]. Using this database, Battalio and Wang [84] found that many northern hemisphere originating sequences flush into the southern hemisphere following more coherent tracks while the sequence paths in the southern hemisphere were less organized.

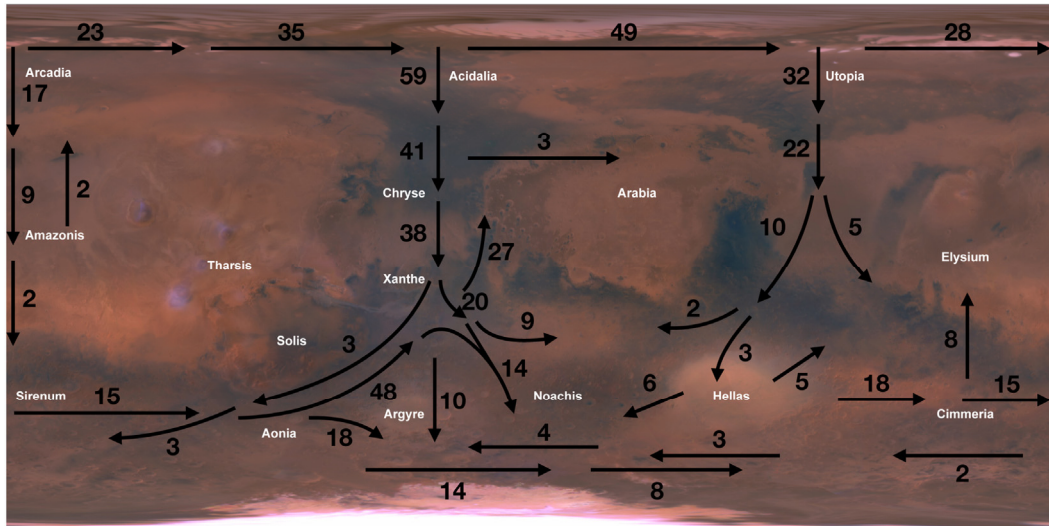


Figure 3. Paths of dust storm sequences observed by MGS MOC and MRO MARCI during Martian year 24 and 32. The numbers near the arrows indicate the number of sequences traveling along that path. (Adapted from Battalio and Wang [84]).

Recently, China's Tianwen-1 orbiter was equipped with a medium resolution camera (MoRIC) [85], which is a standard RGB color camera. The main objective was to photograph the surface of Mars, draw global remote sensing images of Mars, explore the topography of Mars and its changes, and study the geological structure, topography, and landform of Mars. MoRIC had a FOV of $53.3^\circ \times 41.2^\circ$, and the corresponding spatial resolution of nadir point at an orbital altitude of 400 km is about 98 m. Dust storms can be seen directly in the images captured by MoRIC (as shown in Figure 1a).

3.3. Orbiter Infrared Spectroscopy

The visible light images captured by the orbiter cameras can monitor the global distribution and spatiotemporal changes of the dust storms, but there are many difficulties in quantitative inversion of the strengths of dust storm, especially the accurate Martian surface albedo model is required. At present, the main method of quantitative monitoring of dust storms in Mars orbit is to use infrared spectrometers.

Infrared spectrum observations on Mars orbiters have a long history since Mariner 6 & 7 [85,86]. As the infrared spectroscopy and radiative transfer models become mature, starting with the MGS, the NASA's Mars Orbiters is all equipped with infrared/thermal infrared spectrometers to continuously monitor the Martian atmosphere and dust storms, including the thermal infrared spectrometer (TES) on the MGS [87], the Thermal Emission Imaging System (THEMIS) on Odyssey [88], and the Mars Climate Sounder (MCS) aboard the MRO [89]. The three spectrometers together provided continuous and complete quantitative monitoring data of global dust activities on Mars since Martian year 24 (1998–present). Apart from THEMIS, which just adopted nadir viewing mode, both TES and MCS adopted scanning mode to realize nadir and limb observations.

The advantage of limb observation is that the altitudinal profiles of dust storms can be retrieved, as well as other atmospheric parameters, such as temperature profiles and water ice profiles with radiometric information at specific wavelengths. The basic principle for retrieving the dust optical depth (DOD) in infrared is based on the radiative transfer models of Martian atmosphere to search for the optimized profiles of temperature, dust, and water ice to best match the observed radiation profiles. The general radiative transfer equation is [90,91]

$$I_{obs}(\nu) = \epsilon(\nu)B[T_{surf}, \nu]e^{-\frac{\tau_0(\nu)}{\mu}} + \int_0^{\tau_0(\nu)} B[T(\tau), \nu]e^{-\frac{\tau(\nu)}{\mu}} d\tau, \quad (1)$$

where $I_{obs}(\nu)$ is the observed monochromatic radiance of Mars at wave number ν , $\epsilon(\nu)$ is the surface emissivity at wave number ν , $B[T(\tau), \nu]$ is the Planck function, $\tau_0(\nu)$ is the normal column-integrated aerosol optical depth, μ is the cosine of emission angle, T_{surf} is the surface temperature, $T(\tau)$ is the atmospheric temperature, and the integration is performed from the spacecraft to the surface.

The aerosol optical depth is mainly contributed from dust particles, water ice, and CO₂. Hence, $\tau_0(\nu)$ can be factorized to be [92]

$$\tau_0(\nu) = A_{dust}f_{dust}(\nu) + A_{ics}f_{ics}(\nu) + A_{CO_2}f_{CO_2}(\nu) \quad (2)$$

where $f_{dust}(\nu)$, $f_{ics}(\nu)$, and $f_{CO_2}(\nu)$ are the wavelength dependence of dust, water ice, and CO₂ optical depth, and A_{dust} , A_{ics} , and A_{CO_2} are their scaling factors at standard wavelengths, which are 9.3 μm or 21.6 μm for dust, 12 μm for water ice, and 9.3 μm for CO₂, respectively. At these standard wavelengths, $f_{dust}(\nu) \equiv 1$, $f_{ics}(\nu) \equiv 1$, and $f_{CO_2}(\nu) \equiv 1$. Assuming a plane-parallel atmosphere and uniform mixing of dust, water ice, and CO₂, equation (1) can be solved to obtain DOD.

Apparently, DOD obtained with observed radiance at different wave bands should have different values. For example, the 9.3 μm DOD represents the dust-induced absorption at 9.3 μm , while the 21.6 μm DOD represents the dust-induced absorption at 21.6 μm [93]. The 21.6 μm DOD can be converted to 9.3 μm DOD by multiplying a factor of 2.7 [22]. The DOD retrieved from TES, THEMIS, and MCS formed the most important quantitative dust storm database.

3.4. Landers/Rovers Monitoring

On Mars surface, the received solar visible radiations can be used to measure the dust storm activity. According to the Beer-Lambert Law, the solar radiation flux (F) that arrives Mars surface can be expressed as $F = F_{TOA} \times e^{-\tau\eta}$, where τ represents the visible DOD (VDOD), F_{TOA} is the solar radiation flux at the top of atmosphere, and η denotes the atmospheric optical path [94].

In principle, if F_{TOA} and F can be simultaneously measured, the VDOD can be calculated. However, it is almost impossible for synchronous measurements at the top of atmosphere and on the surface along the same line of sight. A smart technique can be used. By taking the logarithm of the Beer-Lambert Law, we get $\ln F = \ln F_{TOA} - \tau\eta$. Assuming that in a certain time range, τ is constant at different solar altitude angle η , we can fit the measured F at different η to obtain the slope τ (VDOD) and the intercept F_{TOA} . This approach was successfully applied on Mars Exploration Rover (MER) Opportunity and Spirit, as well as other landers/rovers. The panoramic cameras on both rovers routinely image the Sun near local noon in each day of Mars at 440 nm and 880 nm [94,95].

The VDOD retrieved from the two wavelengths are almost the same, as shown by the VDOD series during the lifetime of Opportunity rover in Figure 4. The Opportunity rover survived from the 2007 global dust storm but was unfortunately completely lost during the 2018 global dust storm. The images of the Sun taken by Opportunity rover during the eruption of the 2018 global dust storm clearly show the drastic attenuation of solar visible radiations on Mars surface due to the strong absorption of dust particles (Figure 5). When VDOD achieved 11, the visible light can be attenuated by nearly 100%, and the attenuation of infrared band is also 98%, and the surface of Mars becomes dark. It is noted that, the infrared DOD introduced in Section 3.3 can also be converted to VDOD, i.e., the 21.6 μm DOD can be converted to VDOD by multiplying a factor of 7.3, and the 9.3 μm DOD can be converted to VDOD by dividing a factor of 2.7 [22,96].

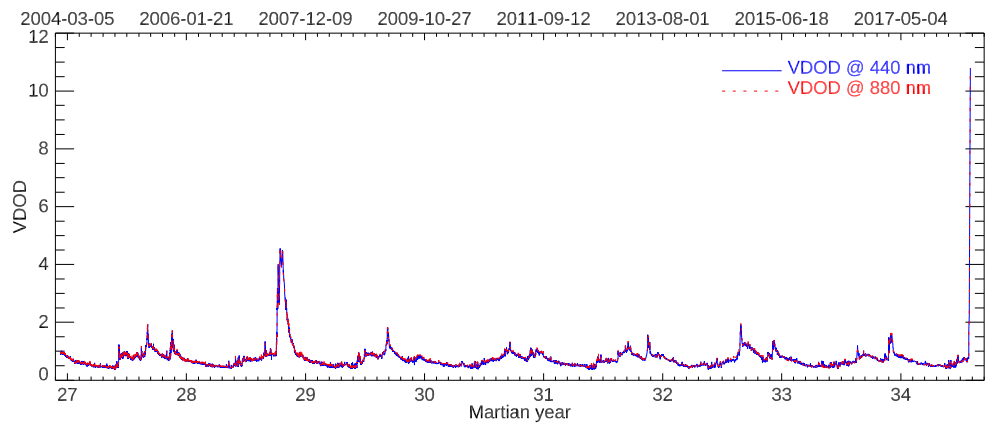


Figure 4. The VDOD recorded by Opportunity rover. VDOD observed in 440 nm (blue solid) and 880 nm (red dashed) are shown.

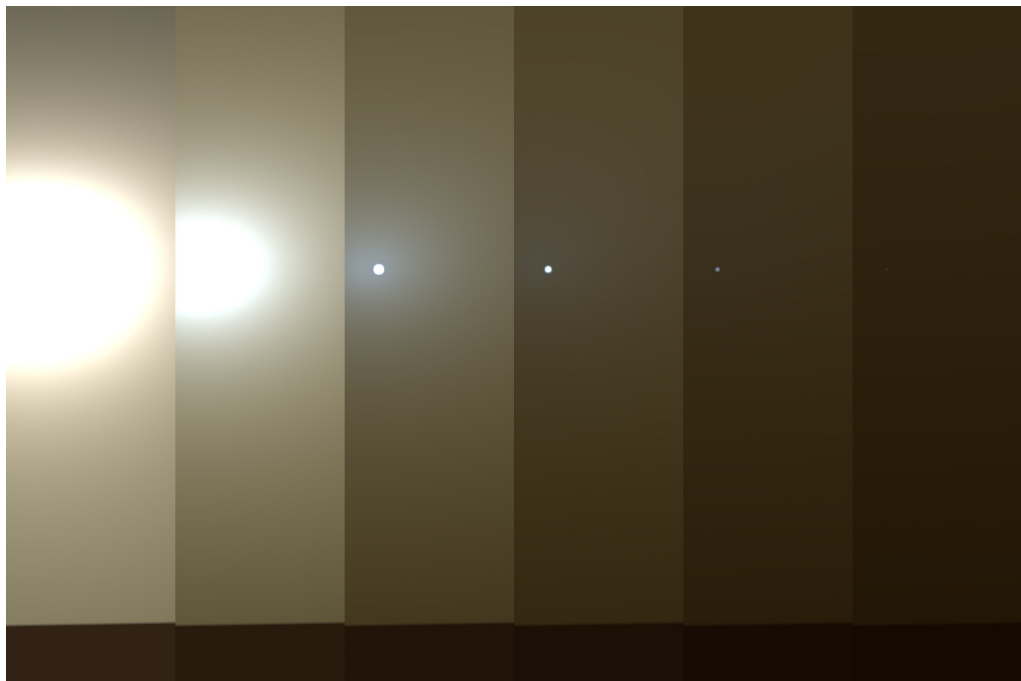


Figure 5. Photographs of the Sun in visible light captured by the panoramic camera onboard Opportunity rover during the eruption phase of the global dust storm in June 2018. The VDOD for each frame is 1, 3, 5, 7, 9, and 11, from left to right. (Image taken from <https://www.jpl.nasa.gov/images/pia22521-shades-of-martian-darkness>, Credit: NASA/JPL-Caltech/TAMU).

Based on the operation status and record for the landers and rovers on Mars during the past two decades, different levels of dust storms have different effects on the landers/rovers, and the engineering team in NASA provided a guidebook for dust storm operation [97]. In this guidebook, the dusk storm was classified into six levels according to the values of VDOD, as listed in Table 1.

Table 1. Classification of dust storm levels according to VDOD [97].

Levels	VDOD Values	Actions
Level 1	<0.7	No restrictions.
Level 2	0.7<VDOD<1.0	No restrictions but watch the VDOD closely.
Level 3	1.0<VDOD<2.0	Scientific activities can only be carried out in reasonable limits during the day, with no overnight

		activities, and the operation team searches for possible parking points for rovers and protective measures for landers.
Level 4	$2.0 < VDOD < 3.0$	Start driving to a parking point to safely ride out the dust storm, allowing ONLY essential activities (VDOD observation and battery control board history).
Level 5	$3.0 < VDOD < 3.5$	Final drive to parking point, minimal activities ONLY (VDOD observation and battery control board history), begin ultra-high frequency (UHF) overflights per couple of days, and wait for VDOD to drop.
Level 6	$VDOD > 3.5$	Minimal activities ONLY (VDOD observation and battery control board history), UHF overflights per couple of days, and wait for VDOD to drop.

It is worth noting that, the developing trend of large dust storms is different, and continuous monitoring and treatment according to the actual situation becomes particularly important. For example, it took 4 days for the VDOD value to increase from 1 to 2 during the 2017 global dust storm, while it took just 1 day during the 2018 global dust storm. The dust storm grew so rapidly that the guidebook must be threw away.

For landers/rovers using solar array as power source, dust storms, especially the global dust storms, can dramatically accelerate the rate of dust deposition, resulting the fast degradation of power supply. The averaged dust factor decrease rate is 0.2% per Martian day [98]. During large dust storms, however, the dust can be seasonally removed owing to the large wind. The loss of solar energy is mainly due to the decrease of solar insolation. During the 2018 global dust storm, when the VDOD values increased from 0.6 to 10.8 in 8 days (Jun 3–10 2018), the solar array energy dropped 96.7% [97]. From Jun 10 on, the Opportunity rover is officially dead, after 15 years of successful exploration on Mars. Earlier in March 2010, another MER rover Spirit was dead after it got stuck in a sand trap. These missions provided us with important lessons that, for exploration activities on Mars surface, seasonal dust storms have great impacts on landers/rovers and real-time monitoring of the dust storm activity from both orbiters and landers/rovers is crucial for the security and successful implementation of scientific explorations.

4. Dust Storm Monitoring and Forecasting for Tianwen-3

China has announced the implementation of Mars sampling returning mission around 2030 [99]. During the whole mission, the entry, descending and landing process, sampling process, and the Martian surface launch process are most likely to be affected by Martian dust storms. In this section, we discuss the possible characteristics of dust storm activity during the Tianwen-3 mission and propose dust monitoring scheme for Tianwen-3.

4.1. Statistical Predictions

Based on the long-term dust storm observation data, mainly the CDOD retrieved from TES, THEMIS, and MCS, Montabone et al. [22,23] carried systematic data processing, cross-calibration, and quality control on these data and established a large DOD database covering Martian year 24 to present. The database is global, with a spatial resolution of 6° (longitude) by 5° (latitude) and a temporal resolution of 1 Martian day. The DOD data in the database are all 9.3 μm CDOD. We converted the 9.3 μm CDOD data to VDOD using the coefficient in Section 3.4 to facilitate the assessment of the degree of dust storm impact according to the classification criteria in Table 1.

Suppose that the sampling will be in flat area in the low latitude regions in the northern hemisphere, we randomly selected four zones in to statistically predict the dust storm levels. The statistical procedure is as following.

- The four zones are in the Utopia Plain, Isidis Basin, Amazon Plain, and Chryse Plain, respectively. Each has a range of 18° in longitude and 15° in latitude, that is a 3×3 grid in the VDOD database;
- The VDOD data in the grid during Martian year 24-35 are extracted from the database to form a subset for this region;
- In each Martian day, the probabilities of the six dust activity levels are then calculated;
- Since Martian dust storms are seasonal, we extend the date to Martian year 40 and 41 according to the orbit of Mars;
- Finally, the predicted results are shown in Figure 6.

Take the zone in Utopian Plain as an example (Figure 6a), it is found that,

- Before southern hemisphere spring equinox ($L_s < 180^\circ$), the dust activity is weak, basically below the safety line ($VDOD < 1.0$), and occasionally higher 1.0 with a very short duration;
- After southern hemisphere spring equinox ($L_s > 180^\circ$), the probability of VDOD exceeding 1.0 increases significantly. Especially between L_s of $200^\circ \sim 240^\circ$ (i.e., October 7 to December 11, 2029 in Martian year 40 and August 25 to October 29, 2031 in Martian year 41), the probability of VDOD exceeding 2.0 is greater than 30%. The dust activity generally peaks near L_s of $210^\circ \sim 220^\circ$, and then begins to weaken and recover. During this period, the operators should pay close attention to the changing trend of dust activity;
- After southern hemisphere summer solstice ($L_s > 270^\circ$), the dust activity is significantly weakened, but still in active level. There is an active period around southern hemisphere autumn equinox ($L_s \sim 270^\circ$), the probabilities for Level 2 and Level 3 are both about 50%. After then, the dust activity will recover to quiet condition and begins another seasonal trend.

In general, before July-September 2029 or May-July 2031, the overall level of Martian dust storms is very low, and it is relatively safe to conduct sampling and returning activities. After July-September 2029 or May-July 2031, a significant increase in regional or global dust activity may have a significant impact on sampling and returning activities. A comparison between different zones in Figure 6 indicates that the dust activity level in higher latitudes is generally lower than that near the equator, and it is recommended to select higher latitudes as far as scientific requirements and engineering technology allow, while completing the relevant science and engineering tasks by July 2029 or May 2031. It's worth noting that Figure 5 is just a preliminary statistical analysis, which can provide a preliminary reference for engineering task planning. However, to minimize the impact of dust storms on the Mars sampling returning mission, it is necessary to establish a Mars dust storm monitoring and early warning system before the implementation of the mission [16].

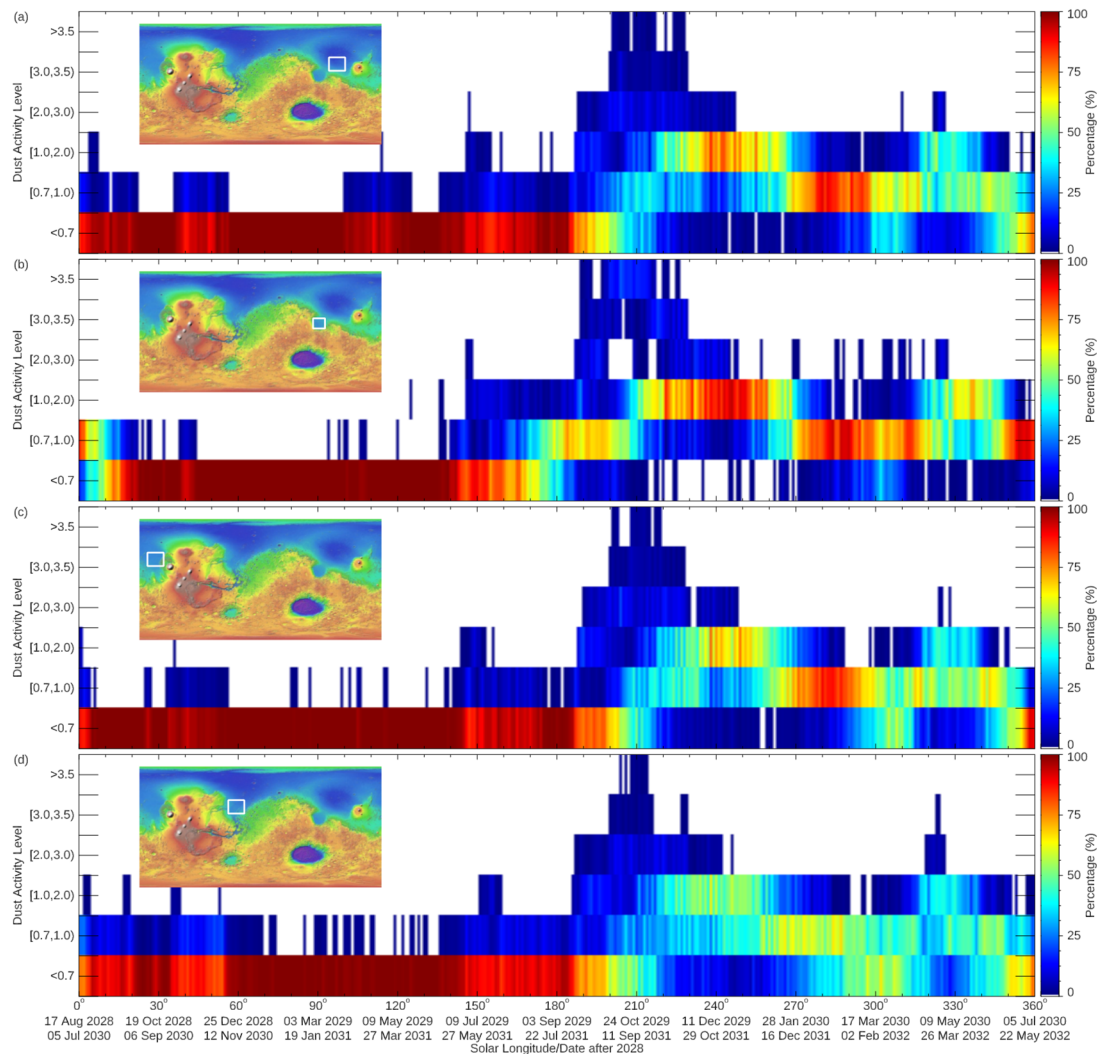


Figure 5. Statistical predictions of the dust storm activity level at five zones in the low-latitude regions of Mars. (a) Utopia Plain, (b) Isidis Basin, (c) Amazon Plain, (d) Chryse Plain. Modified from He et al. [100].

4.2. Dust Storm Monitoring for Tianwen-3

During the sampling and returning mission, there will be an orbiter to provide to provide high resolution mapping of landing site and measurements of environmental parameters, including dust storm activity. We have proposed to carry a Mars Multicolor Camera (MMC) to monitor dust storms. The main scientific objectives of MMC are:

- Martian dust storm monitoring and early warning: Conduct large-field multicolor imaging of mid-low latitude dust storm activities on Mars to obtain information such as location, scope and moving speed of dust storms on Mars.
- Spatial and temporal distribution of atmospheric ozone on Mars: Conduct large-field ultraviolet imaging of the column content of low-latitude ozone on Mars to obtain its spatial and temporal distributions, and to improve the accuracy of dust storm identification in combination of water-ice cloud identification in visible light channels.

The Tianwen-3 orbiter will potentially operate in a polar circular orbit with an altitude of ~350 km, an orbital inclination of ~30°, and an orbital period of ~1.8 hours, making it an ideal orbit for global imaging of Martian dust storms in the middle and low latitudes. At this altitude, a camera with FOV of 130° will achieve the largest surface coverage of ~3000 km cross-track. Considering the rotation of Mars, a global image of Mars will be generated each Martian day, covering an area below

52° latitude, as shown by the white circles in Figure 7. Owing to the combined effects of orbital motion and Mars rotation, the revisit times of the MMC for the same area are shown in Figure 8.

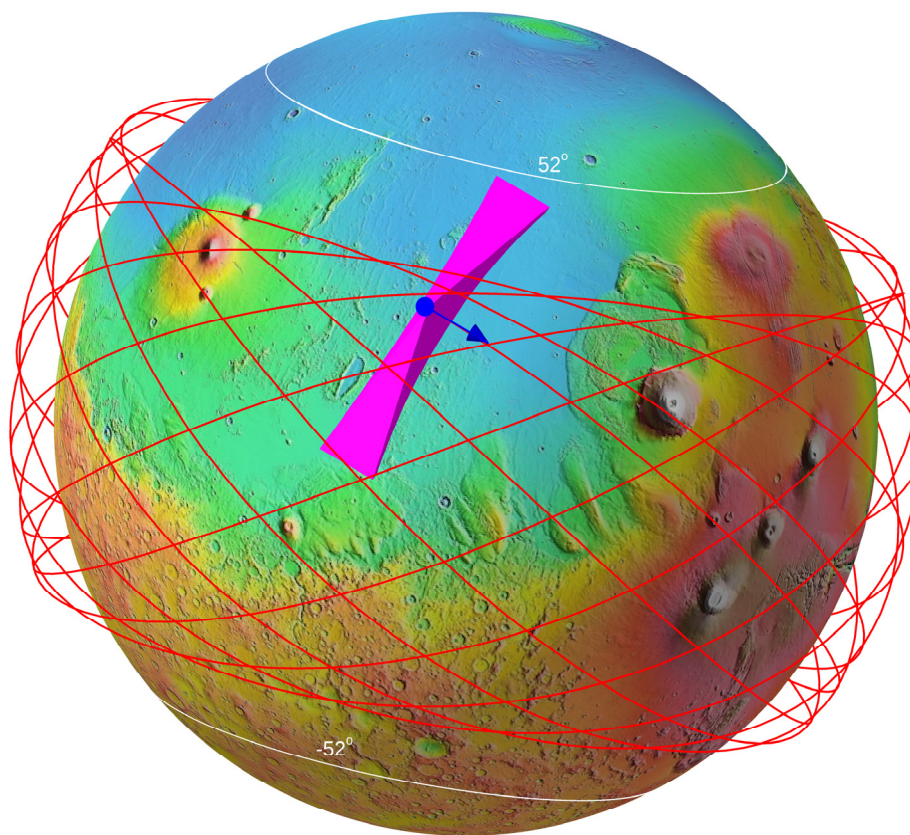


Figure 7. A demo of the orbit of Tianwen-3 orbiter. The orbit is plotted by red lines. The orbiter is denoted by the blue dot with its velocity shown by the blue arrow. The pink surfaces demonstrate the FOV of the MMC. The background Mars digital elevation map is available at the U.S. Geological Survey Astrogeology Science Center (<https://astrogeology.usgs.gov/search/map/Mars/>).

The rotation period of Mars is ~24.62 hours, and the orbital period of the Tianwen-3 orbiter is ~1.8 hours. It is necessary to consider the coverage of the MMC FOV to the same area during the daytime period of each Mars day. As can be seen from Figure 8, during the daytime of each Martian day, an area of about 2000 km × 3000 km below 30° latitude can be continuously observed during six orbits. In other words, for such an area of 2000 km × 3000 km, the MMC can achieve continuous monitoring with a time resolution of better than 2 hours. This is of great significance for the early warning and prediction of sandstorm during the landing sample-return mission.

The revisit rate for different cross-track FOV of MMC is further shown in Figure 8. When the cross-track FOV decrease from 130° (black) to 110° (pink), the area than can be revisited by MMC for six times is significantly shrank. When the cross-track FOV is smaller than 110°, no area can be revisited by six time. Therefore, it is determined that the cross-track FOV of MMC should be larger than 130°. The along-track FOV is not so critical since the MMC will operate in a push frame mode and it will be as small as possible to reduce the data rate. We suggested that, once the landing and sampling site is determined, the tilt of the orbit should be as small as possible, and the orbital phase of the orbiter should be optimized to revisit six times or more above the landing site.

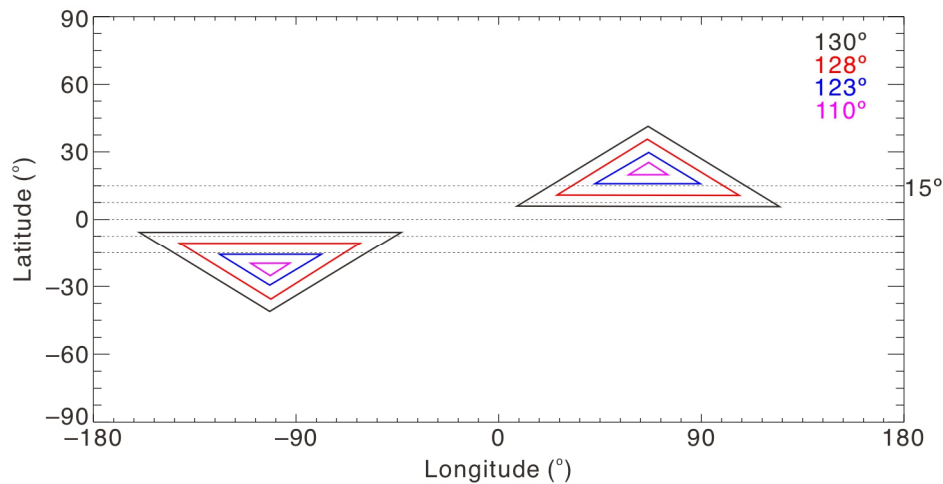


Figure 8. The surface areas that can be revisited by MMC for six times during Martian daytime with different cross-track FOV as shown by different colors.

To achieve the scientific objectives of MMC, the selection of wavelengths is essential. Since the MRO MARCI has been a great success, the operation wavelengths of MMC will be similar to MARCI. We have decided to design seven channels centered at ~260 nm, ~320 nm, ~425 nm, ~550 nm, ~600 nm, ~770 nm, and ~860 nm, respectively. The expected spatial resolution of the MMC images will be 1 km near nadir points. The images of each channel can be used individually to study the Martian atmosphere and surface, such as clouds, circulation, dust swirls and dust storms, atmospheric ozone, polar surface processes, local albedo properties, surface color properties, mineralogical constraints, and surface physical constraints, and can also be used to synthesize different channel colors for the identification of Martian dust storms. For example, the false color RGB composite generated from channels at ~425 nm, ~600 nm and ~600 nm will be to identify the locations, ranges and evolutions of dust storms, and the false color RGB composite generated from channels at ~260 nm, ~320 nm, and ~425 nm is suitable for the identification of ice cloud to further improve the reliability of dust storm identification.

5. Conclusions

Dust storms play a crucial role in the climate system and the space environment of Mars and have a great impact on human's Mars exploration activities. Since the Martian dust storms involve the geological and geochemical processes, the surface chemics and physics processes, the atmospheric chemics and physics processes, the Mars orbital motion, and the solar energy input, advances in the study of the driving mechanism of Martian dust storms and their environmental effects will advance our understanding of the habitable environment on Mars.

At present, the international Mars exploration is in full swing, and will even enter the era of multi-satellite and multi-lander explorations [102]. The basis of in-depth and systematic study of Martian dust storm is to establish a stereo observation network that could quantitatively monitor the three-dimensional spatial distribution and dynamic evolution of the global dust activities on Mars. To truly understand mechanisms that control the outbreak, development, and decline of dust storms and the interannual variation of global dust storms, missions that persistently span as many as local times and latitudes as possible across the lower, middle, and upper atmosphere are required. For orbiters, multicolor cameras and ultraviolet and infrared spectrometers will be valuable. Small multispectral cameras in visible and near infrared bands will be essential for safe and smooth operation of landers and rovers on Mars.

We emphasize on the data-driven simulation works on Martian dust storms. A combination between data assimilation and Mars GCM is a potential solution to better understanding the Martian atmosphere [48,49]. Comparative studies will also be helpful. The Martian dust cycle shares many

analogous characteristics with the water cycle on Earth [48], and comparative studies between them will deepen our understandings on the two sister planets.

Author Contributions: Conceptualization, F.H. and Z.R.; methodology, F.H.; software, F.H.; validation, F.H.; formal analysis, F.H.; investigation, F.H., Z.R., Y.W.; resources, F.H.; data curation, F.H.; writing—original draft preparation, F.H.; writing—review and editing, F.H., Z.R., Z.W., J.G., K.F., X.Z., L.Y., Y.Q.W. and Y.W.; visualization, F.H.; supervision, F.H.; project administration, F.H. and Z.R.; funding acquisition, F.H., and Z.R. All authors have read and agreed to the published version of the manuscript.

Funding: This research was funded by the National Natural Science Foundation of China (42222408, 41931073) and the National Key R&D Program of China (2021YFA0718600). F.H. was supported by the Youth Innovation Promotion Association of the Chinese Academy of Sciences (Y2021027). Z.R. was supported by the Key Research Program of Chinese Academy of Sciences (ZDBS-SSW-TLC00103) and the Key Research Program of the Institute of Geology and Geophysics, CAS (IGGCAS- 202102).

Data Availability Statement: The Opportunity rover visible dust optical depth data are publicly available at https://pds-geosciences.wustl.edu/mer/mer1_mer2-m-pancam-5-atmos-opacity-v1/merao_1xxx/data/. The Mars digital elevation map is publicly available at the U.S. Geological Survey Astrogeology Science Center at <https://astrogeology.usgs.gov/search/map/Mars/>. The Mars dust storm database is publicly available at the Mars Climate Database at https://www-mars.lmd.jussieu.fr/mars/dust_climatology/index.html. The Mars Daily Global Maps are publicly available at https://www.msos.com/view.php?page=subject/weather_reports.

Acknowledgments: The authors thank the Dr. L.Montabone for providing the Mars dust optical depth database.

Conflicts of Interest: The authors declare no conflicts of interest.

References

- Connerney, J.E.P.; Acuña, M.H.; Wasilewski, P.J.; Ness, N.F.; Rème, H.; Mazelle, C.; Vignes, D.; Lin, R.P.; Mitchell, D.L.; Cloutier, P.A. Magnetic lineations in the ancient crust of Mars. *Science*, 1999, 284(5415), 794–798.
- Jakosky, B.M. Atmospheric loss to space and the history of water on Mars. *Ann. Rev. Earth Planet. Sci.* 2021, 49(1), 71–93.
- Chaffin, M.S.; Kass, D.M.; Aoki, S.; Fedorova, A.A.; Deighan, J.; Connour, K.; Heavens, N.G.; Kleinböhl, A.; Jain, S.K.; Chaufray, J.-Y.; Mayyasi, M.; Clarke, J.T.; Stewart, A.I.F.; Evans, J.S.; Stevens, M.H.; McClintock, W.E.; Crismani, M.M.J.; Holsclaw, G.M.; Lefevre, F.; Lo, D.Y.; Montmessin, F.; Schneider, N.M.; Jakosky, B.; Villanueva, G.; Liuzzi, G.; Daerden, F.; Thomas, I.R.; Lopez-Moreno, J.-J.; Patel, M.R.; Bellucci, G.; Ristic, B.; Erwin, J.T.; Vandaale, A.C.; Trokhimovskiy, A.; Korabiev, O.I. Martian water loss to space enhanced by regional dust storms. *Nat. Astronom.* 2021, 5, 1036–1042.
- Dubinin, E.; Fraenz, M.; Pätzold, M.; McFadden, J.; Halekas, J.S.; DiBraccio, G.A.; Connerney, J.E.P.; Eparvier, F.; Brain, D.; Jakosky, B.M.; Vaisberg, O.; Zelenyi, L. The effect of solar wind variations on the escape of oxygen ions from Mars through different channels: MAVEN observations. *J. Geophys. Res. Space Phys.* 2017, 122, 11,285–11,301.
- Heavens, N. G.; Kleinböhl, A.; Chaffin, M. S.; Halekas, J. S.; Kass, D. M.; Hayne, P. O.; McCleese, D.J.; Piqueux, S.; Shirley, J.H.; Schofield, J.T. Hydrogen escape from Mars enhanced by deep convection in dust storms. *Nat. Astronom.* 2018, 2, 126–132.
- Lillis, R.J.; Brain, D.A.; Bougher, S.W.; Leblanc, F.; Luhmann, J.G.; Jakosky, B.M.; Modolo, R.; Fox, J.; Deighan, J.; Fang, X.; Wang, Y.C.; Lee, Y.; Dong, C.; Ma, Y.; Cravens, T.; Andersson, L.; Curry, S.M.; Schneider, N.M.; Combi, M.; Stewart, I.; Clarke, J.; Grebowsky, J.; Mitchell, D.L.; Yelle, R.; Nagy, A.F.; Baker, D.; Lin R.P. Characterizing atmospheric escape from Mars today and through time, with MAVEN. *Space Sci. Rev.* 2015, 195, 357–422.
- Lundin, R.; Barabash, S.; Andersson, H.; Holmström, M.; Grigoriev, A.; Yamauchi, M.; Sauvaud, J.-A.; Fedorov, A.; Dudnik, E.; Thocaven, J.J.; Wingham, D.; Frahm, R.; Scherrer, J.; Sharber, J.; Asamura, K.; Hayakawa, H.; Coates, A.; Linder, D.R.; Curtis, C.; Hsieh, K.C.; Sandel, B.R.; Grande, M.; Carter, M.; Reading, D.H.; Koskinen, H.; Kallio, E.; Riihela, P.; Schmidt, W.; Säles, T.; Kozyra, J.; Krupp, N.; Woch, J.; Luhmann, J.; McKenna-Lawler, S.; Cerulli-Irelli, R.; Orsini, S.; Maggi, M.; Mura, A.; Milillo, A.; Roelof, E.; Williams, D.; Livi, S.; Brandt, P.; Wurz, P.; Bochsler, P. (2004). Solar wind-induced atmospheric erosion at Mars: First results from ASPERA-3 on Mars Express. *Science*, 305, 1933–1936
- Ramstad, R.; Barabash, S.; Futaana, Y.; Nilsson, H.; Wang, X.-D.; Holmström, M. The Martian atmospheric ion escape rate dependence on solar wind and solar EUV conditions: 1. Seven years of Mars Express observations. *J. Geophys. Res. Planet.* 2015, 120, 1298–1309

9. Wei, Y.; Fraenz, M.; Dubinin, E.; Woch, J.; Lühr, H.; Wan, W.; Zong, Q.-G.; Zhang, T.L.; Pu, Z.Y.; Fu, S.Y.; Barabash, S.; Lundin, R.; Dandouras, I. (2012). Enhanced atmospheric oxygen outflow on Earth and Mars driven by a corotating interaction region. *J. Geophys. Res.* 2012, 117, A03208.
10. Barlow, N. *Mars: An Introduction to Its Interior, Surface and Atmosphere*. Cambridge University Press: New York, USA, 2008; pp. 163–186.
11. Leovy, C. Weather and climate on Mars. *Nature*, 2001, 412, 245–249.
12. Shirley, J.H. Solar system dynamics and global-scale dust storms on Mars. *Icarus*, 2015, 251, 128–144.
13. Schmidt, F.; Way, M.J.; Costard, F.; Bouley, S.; Séjourné, A.; Aleinov, I. Circumpolar ocean stability on Mars 3 Gy ago. *Proc. Natl. Acad. Sci. USA* 2022, 119, e2112930118.
14. Wei, Y.; He, F.; Fan, K.; Rong, Z.; Wang, Y. Preliminary predictions of the dust storm activity at the landing site of China's Zhurong Mars rover in 2022 (in Chinese). *Chin. Sci. Bull.* 2022, 67, 1938–1944.
15. Wang, Y.; Wei, Y.; Fan, K.; He, F.; Rong, Z.; Zhou, X.; Tan, N. The impact of dust storms on Mars surface rovers: Review and prospect (in Chinese). *Chin. Sci. Bull.* 2023, 68, 368–379.
16. Rong, Z.; Wei, Y.; He, F.; Gao, J.; Fan, K.; Wang, Y.; Cao, L.; Yan, L.; Ren, Z.; Zhou, X.; Tan, N.; Yu, T. The orbit schemes to monitor Martian dust storms: Benefits to China's future mars missions (in Chinese). *Chin. Sci. Bull.* 2023, 68, 716–728.
17. Martin, L.J.; Zurek, R.W. An analysis of the history of dust activity on Mars. *J. Geophys. Res.* 1993, 98, 3221–3246.
18. Cantor, B.A.; James, P.B.; Caplinger, M.; Wolff, M.J. Martian dust storms: 1999 Mars Orbiter Camera observations. *J. Geophys. Res.* 2001, 106, 23653–23688.
19. Wang, H.; Richardson, M.I. The origin, evolution, and trajectory of large dust storms on Mars during Mars Year 24–30 (1999–2011). *Icarus* 2015, 251, 112–127.
20. Sánchez-Lavega, A.; del Río-Gaztelurrutia, T.; Hernández-Bernal, J.; Delcroix, M. The onset and growth of the 2018 Martian Global Dust Storm. *Geophys. Res. Lett.* 2019, 46, 6101–6108.
21. Kass, D.M.; Kleinböhl, A.; McCleese, D.J.; Schofield, J.T.; Smith, M.D. Interannual similarity in the Martian atmosphere during the dust storm season. *Geophys. Res. Lett.* 2016, 43, 6111–6118.
22. Montabone, L.; Forget, F.; Millour, E.; Wilson, R.J.; Lewis, S.R.; Cantor, B.; Kass, D.; Kleinböhl, A.; Lemmon, M.T.; Smith, M.D.; Wolff, M.J. Eight-year climatology of dust optical depth on Mars. *Icarus* 2015, 251, 65–95.
23. Montabone, L.; Spiga, A.; Kass, D.M.; Kleinböhl, A.; Forget, F.; Millour, E.. Martian year 34 column dust climatology from Mars Climate Sounder observations: Reconstructed maps and model simulations. *J. Geophys. Res. Planet.* 2020, 125, e2019JE006111.
24. Lemmon, M.T.; Guzewich, S.D.; McConnochie, T.; de Vicente-Retortillo, A.; Martínez, G.; Smith, M.D.; Bell III, J.F.; Wellington, D.; Jacob, S. Large dust aerosol sizes seenduring the 2018 Martian global dust event by the Curiosity rover. *Geophys. Res. Lett.* 2019, 46, 9448–9456.
25. Chen-Chen, H.; Pérez-Hoyos, S.; Sánchez-Lavega, A. Dust particle size, shape and optical depth during ht e2018/MY34 martian global dust storm retrieved by MSL Curiosity rover Navigation Cameras. *Icarus* 2021, 354, 114021.
26. Clancy, R.T.; Wolff, M.J.; Christensen, P.R. Mars aerosol studies with the MGS TES emission phase function observations: Optical depths, particle sizes, and ice cloud types versus latitude and solar longitude. *J. Geophys. Res.* 2003, 108, 5098.
27. Wolff, M.J.; Clancy, R.T. Constraints on the size of Martian aerosols from thermal emission spectrometer observations. *J. Geophys. Res.* 2003, 108(E9), 5097.
28. Vicente-Retortillo, Á.; Martínez, G.; Rennó, N.; Lemmon, M.T.; de la Torre Juarez, M. Determination of dust aerosol particle size at Gale crater using REMS UVS and Mastcam measurements. *Geophys. Res. Lett.* 2017, 44, 3502–3508.
29. Fedorova, A.A.; Montmessin, F.; Rodin, A.V.; Korablev, O.I.; Maattanen, A.; Maltagliati, L.; Bertaux, J.-L. Evidence for a bimodal size distribution for the suspended aerosol particles on Mars. *Icarus* 2014, 231, 239–260.
30. Guzewich, S.D.; Tiogo, A.D.; Richardson, M.I.; Newman, C.E.; Talaat, E.R.; Waugh, D.W.; McConnochie, T.H. The impact of a realistic vertical dust distribution on the simulation of the Martian General Circulation. *J. Geophys. Res. Planet.* 2013, 118, 980–993.
31. Medvedev, A.S.; Yiğit, E.; Kuroda, T.; Hartogh, P. General circulation modeling of the Martian upper atmosphere during global dust storms. *J. Geophys. Res. Planet.* 2013, 118, 2234–2246.
32. Hanel, R.; Conrath, B.; Hovis, W.; Kunde, V.; Lowman, P.; Maguire, W.; Pearl, J.; Pirraglia, J.; Prabhakara, C.; Schlachman, B.; Levin, G.; Straat, P.; Burke, T. Investigation of the Martian environment by infrared spectroscopy on Mariner 9. *Icarus* 1972, 17, 423–442.
33. Leovy, C.B.; Zurek, R.W.; Pollack, J.B. Mechanisms for Mars dust storms. *J. Atmos. Sci.* 1973, 30, 749–762.
34. Gierasch, P.J.; Goody, R.M. A model of a Martian great dust storm. *J. Atmos. Sci.* 1973, 30, 169–179.
35. Leovy, C.B.; Briggs, G.A.; Young, A.T.; Smith, B.A.; Pollack, J.B.; Shipley, E.N.; Wildey, R.L. The Martian atmosphere: Mariner 9 television experiment progress report. *Icarus* 1972, 17, 373–393.

36. Cross, C.A. Heat balance of the Martian polar caps. *Icarus* 1971, 110–114.
37. Ryan, J.A.; Sharman, R.D.; Lucich, R.D. Local Mars dust storm generation mechanism. *Geophys. Res. Lett.* 1981, 8, 899–901.
38. Newman, C.E.; Lewis, S.R.; Read, S.R.; Forget, F. Modeling the Martian dust cycle, 1, Representations of dust transport processes. *J. Geophys. Res.* 2002, 107(E12), 5123.
39. Newman, C.E.; Lewis, S.R.; Read, S.R.; Forget, F. Modeling the Martian dust cycle, 2, Multiannual radiatively active dust transport simulations. *J. Geophys. Res.* 2002, 107(E12), 5124.
40. Ryan, J.A.; Lucich, R.D. Possible dust devils, vortices on Mars. *J. Geophys. Res.* 1983, 88, 11005–11011.
41. Basu, S.; Wilson, J.; Richardson, M.; Ingersoll, A. Simulation of spontaneous and variable global dust storms with the GFDL Mars GCM. *J. Geophys. Res.* 2006, 111, E09004.
42. Shirley, J.H. Solar system dynamics and global-scale dust storms on Mars. *Icarus* 2015, 251, 128–144.
43. Shirley, J.H.; Mischna, M.A. Orbit-spin coupling and the interannual variability of global-scale dust storm occurrence on Mars. *Planet. Space Sci.* 2017, 139, 37–50.
44. Mischna, M.A.; Shirley, J.H. Numerical modeling of orbit-spin coupling accelerations in a Mars general circulation model: Implications for global dust storm activity. *Planet. Space Sci.* 2017, 141, 45–72.
45. Newman, C.E.; Lee, C.; Mischna, M.A.; Richardson, M.I.; Shirley, J.H. An initial assessment of the impact of postulated orbit-spin coupling on Mars dust storm variability in fully interactive dust simulations. *Icarus* 2019, 317, 649–668.
46. Shirley, J.H.; McKim, R.J.; Battalio, J.M.; Kass, D.M. Orbit-Spin Coupling and the Triggering of the Martian Planet-Encircling Dust Storm of 2018. *J. Geophys. Res. Planet.* 2020, 125, e2019JE006077.
47. Bertrand, T.; Wilson, R.J.; Kahre, M.A.; Urata, R.; Kling, A. Simulation of the 2018 global dust storm on Mars using the NASA Ames Mars GCM: A multitracer approach. *J. Geophys. Res. Planet.* 2020, 125, e2019JE006122.
48. Wu, Z.; Li, T.; Heavens, N.G.; Newman, C.E.; Richardson, M.I.; Yang, C.; Li, J.; Cui, J. Earth-like thermal and dynamical coupling processes in the Martian climate system. *Earth Sci. Rev.* 2022, 229, 104023.
49. Zhou, X.; Wei, Y.; Wu, Z.; Ren, Z.; Tan, N.; Fan, S.; He, F.; Rong, Z.; Yan, L.; Wang, Y.; Fan, K.; Gao, J. Martian whole atmosphere model and dust activities: Review and prospect (in Chinese). *Chin. Sci. Bull.* 2024, 69, 1058–1067.
50. Fenton, L.K.; Geissler, P.E.; Haberle, R.M. Global warming and climate forcing by recent albedo changes on Mars. *Nature* 2007, 446, 646–649.
51. Kass, D.M.; Schofield, J.T.; Kleinböhl, A.; McCleese, D.J.; Heavens, N.G.; Shirley, J.H.; Steele, L.J. Mars Climate Sounder observation of Mars' 2018 global dust storm. *Geophys. Res. Lett.* 2020, 47, e2019GL083931.
52. Guzewich, S.D.; Lemmon, M.; Smith, C.L.; Martínez, G.; de Vicente-Retortillo, Á.; Newman, C.E.; Baker, M.; Campbell, C.; Cooper, B.; Gómez-Elvira, J.; Harri, A.-M.; Hassler, D.; Martin-Torres, F.J.; McConnochie, T.; Moores, J. E.; Kahanpää, H.; Khayat, A.; Richardson, M. I.; Smith, M.D.; Sullivan, R.; de la Torre Juárez, M.; Vasavada, A.R.; Viúdez-Moreiras, D.; Zeitlin, C.; Mier, M.-P.Z.. Mars Science Laboratory observations of the 2018/Mars year 34 global dust storm. *Geophys. Res. Lett.* 2019, 46, 71–79.
53. Haberle, R.M.; Pollack, J.B.; Barnes, J.R.; Zurek, R.W.; Leovy, C.B.; Murphy, J.R.; Lee, H.; Schaeffer, J. Mars atmospheric dynamics as simulated by the NASA Ames General Circulation Model: 1. The zonal-mean circulation. *J. Geophys. Res.* 1993, 98(E2), 3093–3123.
54. Wu, Z.; Li, T.; Zhang, X.; Li, J.; Cui, J. Dust tides and rapid meridional motions in the Martian atmosphere during major dust storms. *Nat. Commun.* 2020, 11, 614.
55. Zhao, Y.; Zhong, L.; Yuan, R.; Zhao, C.; Li, R.; Wang, Y.; Lian, Y.; Richardson, M. Simulation of Martian dust effects on polar CO₂ ice caps and atmospheric circulation using the MarsWRF model. *J. Geophys. Res. Planet.* 2021, 126(12), e2021JE006937.
56. Clancy, R.T.; Wolff, M.J.; Lefèvre, F.; Cantor, B.A.; Malin, M.C.; Smith, M.D. Daily global mapping of Mars ozone column abundances with MARCI UV band imaging. *Icarus* 2016, 266, 112–133.
57. Melnik, O.; Parrot, M. Electrostatic discharge in Martian dust storms. *J. Geophys. Res.* 1998, 103, 29107–29117.
58. Farrell, W.M.; Kaiser, M.L.; Desch, M.D.; Houser, J.G.; Cummer, S.A.; Wilt, D.M.; Landis, G.A. Detecting electrical activity from Martian dust storms. *J. Geophys. Res.* 1999, 104, 3795–3801.
59. Krauss, C.E.; Horanyi, M.; Robertson, S. Experimental evidence for electrostatic discharging of dust near the surface of Mars. *New J. Phys.* 2003, 5, 70.
60. Merrison, J.; Jensen, J.; Kinch, K.; Mugford, R.; Nørnberg, P. The electrical properties of Mars analogue dust. *Planet Space Sci.* 2004, 52, 279–290.
61. Michael, M.; Tripathi, S.N. Effect of charging of aerosols in the lower atmosphere of Mars during the dust storm of 2001. *Planet Space Sci.* 2008, 56, 1696–1702.
62. Haider, S.A.; Sheel, V.; Smith, M.D.; Maguire, W.C.; Molina-Cuberos, G.J. Effect of dust storms on the D region of the Martian ionosphere: Atmospheric electricity. *J. Geophys. Res. Space Phys.* 2010, 115, A12336.
63. McDunn, T.L.; Bougher, S.W.; Murphy, J.; Smith, M.D.; Forget, F.; Bertaux, J.-L.; Montmessin, F. Simulating the density and thermal structure of the middle atmosphere (80–130 km) of Mars using the MGCM–MTGCM: a comparison with MEX/SPICAM observations. *Icarus* 2010, 206, 5–17.

64. Chaufray, J.Y.; Chaffin, M.S.; Deighan, J.; Jain, S.; Schneider, N.; Mayyasi, M.; Jakosky, B. Effect of the 2018 Martian global dust storm on the CO₂ density in the lower nightside thermosphere observed from MAVEN/IUVS Lyman-alpha absorption. *Geophys. Res. Lett.* 2020, 47, e2019GL082889.
65. Fang, X.; Ma, Y.; Lee, Y.; Bougher, S.; Liu, G.; Benna, M.; Mahaffy, P.; Montabone, L.; Pawlowski, D.; Dong, C.; Dong, Y.; Jakosky, B. Mars dust storm effects in the ionosphere and magnetosphere and implications for atmospheric carbon loss. *J. Geophys. Res. Space Phys.* 2020, 125, e2019JA026838.
66. Niu, D.D.; Cui, J.; Wu, S.Q.; Gu, H.; Cao, Y.-T.; Wu, Z.-P.; Wu, X.-S.; Zhong, J.-H.; Wu, M.-Y.; Wei, Y.; Zhang, T.-L. Species-dependent response of the Martian ionosphere to the 2018 global dust event. *J. Geophys. Res. Planets.* 2021, 126(2), e2020JE006679.
67. Mukundan, V.; Thampi, S.V.; Bhardwaj, A.; Fang, X. Impact of the 2018 Mars global dust storm on the ionospheric peak: A study using a photochemical model. *J. Geophys. Res. Planet.* 2021, 126, e2021JE006823.
68. Stone, S.W.; Yelle, R.V.; Benna, M.; Lo, D.Y.; Elrod, M.K.; Mahaffy, P.R. Hydrogen escape from Mars is driven by seasonal and dust storm transport of water. *Science* 2020, 370(6518), 824–831.
69. Hvidberg, C.S.; Fishbaugh, K.E.; Winstrup, M.; Svensson, A.; Byrne, S.; Herkenhoff, K.E. Reading the climate record of the Martian polar layered deposits. *Icarus* 2012, 221, 405–419.
70. Colaprete, A.; Barnes, J.; Haberle, R.; Hollingsworth, J.L.; Kieffer, H.H.; Titus, T.N. Albedo of the south pole on Mars determined by topographic forcing of atmosphere dynamics. *Nature* 2005, 435, 184–188.
71. Golombek, M.P.; Warner, N.H.; Ganti, V.; Lamb, M.P.; Parker, T.J.; Ferguson, R.L.; Sullivan, R. Small crater modification on Meridiani Planum and implications for erosion rates and climate change on Mars. *J. Geophys. Res. Planet.* 2014, 119, 2522–2547.
72. Farley, K.A.; Malespin, C.; Mahaffy, P.; Grotzinger, J.P.; Vasconcelos, P.M.; Milliken, R.E.; Malin, M.; Edgett, K.S.; Pavlov, A.A.; Hurowitz, J.A.; Grant, J.A.; Miller, H.B.; Arvidson, R.; Beegle, L.; Calef, F.; Conrad, P.G.; Dietrich, W.E.; Eigenbrode, J.; Gellert, R.; Gupta, S.; Hamilton, V.; Hassler, D.M.; Lewis, K.W.; McLennan, M.; Ming, D.; Navarro-González, R.; Schwenzer, S.P.; Steele, A.; Stolper, E.M.; Sumner, D.Y.; Vaniman, D.; Vasavada, A.; Williford, K.; Wimmer-Schweingruber, R.F.; the MSL Science Team. In Situ Radiometric and Exposure Age Dating of the Martian Surface. *Science* 2013, 343, 1247166.
73. Team R. Characterization of the Martian Surface Deposits by the Mars Pathfinder Rover, Sojourner. *Science* 1997, 278, 1765–1767.
74. Rieder, R.T.; Economou, T.E.; Wänke, H.; Turkevich, A.; Crisp, J.; Brückner, J.; Dreibus, G.; McSween, Jr., H.Y. The Chemical Composition of Martian Soil and Rocks Returned by the Mobile Alpha Proton X-ray Spectrometer: Preliminary Results from the X-ray Mode. *Science* 1998, 278(5344), 1771–1774.
75. Lorenz, R.D.; Martínez, G.M.; Spiga, A.; Vicente-Retortillo, A.; Newman, C.E.; Murdoch, N.; Forget, F.; Millour, E.; Pierron, T. Lander and rover histories of dust accumulation on and removal from solar arrays on Mars. *Planet. Space Sci.* 2021, 207, 105337.
76. Yen, A.; Gellert, R.; Schröder, C.; Morris, R.V.; Bell III, J.F.; Knudson, A.T.; Clark, B.C.; Ming, D.M.; Crisp, J.A.; Arvidson, R.E.; Blaney, D.; Brückner, J.; Christensen, P.R.; DesMarais, D.J.; de Souza Jr, P.A.; Economou, T.E.; Ghosh, A.; Hahn, B.C.; Herkenhoff, K.E.; Haskin, L.A.; Hurowitz, J.A.; Joliff, B.L.; Johnson, J.R.; Klingelhöfer, G.; Madsen, M.B.; McLennan, S.M.; McSween, H.Y.; Richter, L.; Rieder, R.; Rodionov, D.; Soderblom, L.; Squyres, S.W.; Tosca, N.J.; Wang, A.; Wyatt, M.; Zipfel, J. An integrated view of the chemistry and mineralogy of Martian soils. *Nature* 2005, 436, 49–54.
77. Slipher, E.C. *Mars—The Photographic Story*. Northland Press: Arizona, USA, 1962.
78. Martin, L.J.; Zurek, R.W. An analysis of the history of dust activity on Mars. *J. Geophys. Res.* 1993, 98, 3221–3246.
79. Zurek, R.W.; Martin, L.J. Interannual variability of planet-encircling dust storms on Mars. *J. Geophys. Res.* 1993, 98, 3247–3259.
80. Malin, M.C.; Danielson, G.E.; Ravine, M.A.; Soulanille, T.A. Design and development of the Mars Observer Camera. *Int. J. Imaging Syst. Technol.* 1991, 3, 76–91.
81. Malin, M.C.; Danielson, G.E.; Ingersoll, A.P.; Masursky, H.; Veverka, J.; Ravine, M.A.; Soulanille, T.A. Mars Observer Camera, *J. Geophys. Res.* 1992, 97, 7699–7718.
82. Bell III, J.F.; Wolff, M.J.; Malin, M.C.; Calvin, W.M.; Cantor, B.A.; Caplinger, M.A.; Clancy, R.T.; Edgett, K.S.; Edwards, L.J.; Fahle, J.; Ghaemi, F.; Haberle, R.M.; Hale, A.; James, P.B.; Lee, S.W.; MaConnachie, T.; Noe Dobrea, E.; Ravine, M.A.; Schaeffer, D.; Supulver, K.D.; Thomas, P.C. Mars Reconnaissance Orbiter Mars Color Imager (MARCI): Instrument description, calibration, and performance. *J. Geophys. Res.* 2009, 114, E08S92.
83. Li, B.; Yue, Z.; Qu, S.; Yao, P.; Fu, X.; Ling, Z.; Chen, S. Spatio-Temporal Analysis of Dust Storm Activity in Chryse Planitia Using MGS-MOC Observations from Mars Years 24–28. *Universe* 2021, 7, 433.
84. Battalio, M.; Wang, H. The Mars Dust Activity Database (MDAD): A comprehensive statistical study of dust storm sequences. *Icarus* 2021, 354, 114059.
85. Yu, G.B.; Liu, E.H.; Liu, G.L.; Zhou, L.; Zeng J.Z.; Chen, Y.P.; Zhou, X.D.; Zhao R.J.; Zhu, S.Y. Moderate Resolution Imaging Camera (MoRIC) of China's First Mars Mission Tianwen-1. *Earth Planet Phys.* 2020, 4: 364–370.

86. Horn, D.; McAfee, J.M.; Winer, A.M.; Herr, K.C.; Pimentel, G.C. The composition of the Martian atmosphere: Minor constituents. *Icarus* 1972, 16, 543–556.
87. Cimino, G.; Clavin, W.M. Calibration and analysis of Mariner 7 infrared spectra. *Bull. Am. Astron. Soc.* 1996, 28, 1068.
88. Christensen, P.R.; Bandfield, J.L.; Hamilton, V.E.; Ruff, S.W.; Kieffer, H.H.; Titus, T.N.; Malin, M.C.; Morris, R.V.; Lane, M.D.; Clark, R.L.; Jakosky, B.M.; Mellon, M.T.; Pearl, J.C.; Conrath, B.J.; Smith, M.D.; Clancy, R.T.; Kuzmin, R.O.; Roush, T.; Mehall, G.L.; Gorelick, N.; Bender, K.; Murray, K.; Dason, S.; Greene, E.; Silverman, S.; Greenfield, G. Mars Global Surveyor Thermal Emission Spectrometer experiment: Investigation description and surface science results. *J. Geophys. Res.* 2001, 106, 23823–23871.
89. Christensen, P.R.; Jakosky, B.M.; Kieffer, H.H.; Malin, M.C.; McSween Jr., H.Y.; Neelson, K.; Mehall, G.L.; Silverman, S.H.; Ferry, S.; Caplinger, M.; Ravine, M. The Thermal Emission Imaging System (THEMIS) for the Mars 2001 Odyssey mission. *Space Sci. Rev.* 2004, 110, 85–130.
90. McCleese, D.J.; Schofield, J.T.; Taylor, F.W.; Calcutt, S.B.; Foote, M.C.; Kass, D.M.; Leovy, C.B.; Paige, D.A.; Read, P.L.; Zurek, R.W. Mars Climate Sounder: An investigation of thermal and water vapor structure, dust and condensate distributions in the atmosphere, and energy balance of the polar regions. *J. Geophys. Res.* 2007, 112, E05S06.
91. Smith, M.D.; Pearl, J.C.; Conrath, B.J.; Christensen, P.R. Mars Global Surveyor Thermal Emission Spectrometer (TES) observations of dust opacity during aerobraking and science phasing. *J. Geophys. Res.* 2000, 105, 9539–9552.
92. Smith, M.D.; Bandfield, J.L.; Christensen, P.R.; Richardson, M.I. Thermal Emission Imaging System (THEMIS) infrared observations of atmospheric dust and water ice cloud optical depth. *J. Geophys. Res.* 2003, 108, 5115.
93. Smith, M.D. Interannual variability in TES atmospheric observations of Mars during 1999–2003. *Icarus* 2004, 167, 148–165.
94. Kleinböhl, A.; Schofield, J.T.; Kass, D.M.; Abdou, W.A.; Backus, C.R.; Sen, B.; Shirley, J.H.; Lawson, W.G.; Richardson, M.I.; Taylor, F.W.; Teanby, N.A.; McCleese, D.J. Mars Climate Sounder limb profile retrieval of atmospheric temperature, pressure and dust and water ice opacity. *J. Geophys. Res.* 2009, 114, E10006.
95. Lemmon, M.T.; Wolff, M.J.; Bell III, J.F.; Smith, M.D.; Cantor, B.A.; Smith, P.H. Dust aerosol, clouds, and the atmospheric optical depth record over 5 Mars years of the Mars Exploration Rover mission. *Icarus* 2015, 251, 96–111.
96. Bell III, J.F.; Squyres, S.W.; Herkenhoff, K.E.; Maki, J.N.; Arneson, H.M.; Brown, D.; Collins, S.A.; Dingizian, A.; Elliot, S.T.; Hagerott, E.C.; Hayes, A.G.; Johnson, M.J.; Johnson, J.R.; Joseph, J.; Kinch, K.; Lemmon, M.T.; Morris, R.V.; Scherr, L.; Schwochert, M.; Shepard, M.K.; Smith, G.H.; Sohl-Dickstein, J.N.; Sullivan, R.J.; Sullivan, W.T.; Wadsworth, M. Mars Exploration Rover Athena Panoramic Camera (Pancam) investigation. *J. Geophys. Res.* 2003, 108, 8063.
97. Kleinböhl, A.; Schofield, J.T.; Abdou, W.A.; Irwin, P.G.J.; de Kok, R.J. A single-scattering approximation for infrared radiative transfer in limb geometry in the Martian atmosphere. *J. Quant. Spectrosc. Radiat. Transfer.* 2011, 112, 1568–1580.
98. Staab, M.S.; Herman, J.A.; Reich, K.; Reich, K.; Sridhar, V.; Nelson, R.W. MER Opportunity dust-storm recovery operations and implications for future Mars surface missions. In 2020 IEEE Aerospace Conference, Big Sky, MT, USA, 07–14 March 2020.
99. Lorenz, R.D.; Martínez, G.M.; Spiga, A.; Vicente-Retorillo, A.; Newman, C.E.; Murdoch, N.; Forget, F.; Millour, E.; Pierron, T. Lander and rover histories of dust accumulation on and removal from solar arrays on Mars. *Planet Space Sci.* 2021, 207, 105337.
100. Information Office of the State Council of the People's Republic of China. China's Spaceflight in 2021 (in Chinese). Beijing: People's Publishing House, 2022.
101. He, F.; Wei, Y.; Rong, Z.; Reng, Z.; Yan, L.; Tan, N.; Wang, Y.; Fan, K.; Zhou, X.; Gao, J. Monitoring methods for Martian dust storms (in Chinese). *Chin. Sci. Bull.* 2023, 68, 2046–2057.
102. Fan, K.; Wei, Y. Prospection of multi-spacecraft planetary exploration missions in upcoming future (in Chinese). *Chin. Sci. Bull.* 2021, 66, 4350–4353.

Disclaimer/Publisher's Note: The statements, opinions and data contained in all publications are solely those of the individual author(s) and contributor(s) and not of MDPI and/or the editor(s). MDPI and/or the editor(s) disclaim responsibility for any injury to people or property resulting from any ideas, methods, instructions or products referred to in the content.